June 2020

e-NVH Response Synthesis of Electric Motors Based on Stator Teeth FRF Measurements

Raphaël PILE [a,b,c,1], Jean LE BESNERAIS [a], Emile DEVILLERS [a], and Karine DEGRENDELE [a]

[a] *EOMYS ENGINEERING, Lille-Hellemmes 59260, France*
[b] *Univ. Lille, Arts et Metiers ParisTech, Centrale Lille, HEI, EA 2697 - L2EP -Laboratoire d'Electrotechnique et d'Electronique de Puissance, F-59000 Lille, France*
[c] *Univ. Artois, EA 4025, Laboratoire Systèmes Électrotechniques et Environnement (LSEE), F-62400 Béthune, France*

Abstract. The analysis of noise and vibrations under electromagnetic excitations (e-NVH) in electrical machines requires to study the stator mechanical response when excited by Maxwell stress waves. In particular, the notion of unit-wave Frequency Response Function (FRF) is often used in e-NVH simulations to model the mechanical response under electromagnetic excitations and troubleshoot noise issues. However, it is not possible to directly measure the unit-wave FRF on the electrical machines and validate the model. Instead, the Experimental Modal Analysis (EMA) is often compared to a Finite Element (FE) model in order to fit the numerical parameters (damping, boundary conditions, etc.). This paper is presenting a complementary approach to fully numerical e-NVH analysis. It is a new hybrid methodology based on experiments for the mechanical FRF and simulation for the magnetic excitations. This is performed with dedicated experimental measurements and post-processing. The new methodology builds an equivalent unit-wave FRF from experimental measurements. The methodology is validated with the diagnose of electromagnetic noise issues for an experimental benchmark Surface Permanent Magnet Synchronous Machine (SPMSM).

Keywords. Magneto-mechanical analysis, electrical machine, vibration, SPMSM, magnetic force, frequency response function.

[1]Corresponding Author: Raphaël Pile, Eomys Engineering (Lille-Hellemes, France) & Univ. Artois - LSEE (Béthune, France) & Univ. Lille - L2EP (Lille, France); E-mail:raphael.pile@eomys.com.

1. Introduction

Electromagnetic noise and vibration prediction in electrical machine design (e-NVH) is of increasing interest with the widespread use of electric motors. Nevertheless, the magneto-mechanical coupling for numerical simulation is still an active research topic. In particular this article focuses on the methods which allow to include Frequency Response Functions (FRF) [1] in the e-NVH process. The FRF characterizes the response of a given structure to a given load over a whole frequency range. The FRF can be performed through harmonic Finite Element Analysis (FEA) or experimental measurements for example using hammer shocks, sweeping frequency vibrating shaker, etc.

Only the transfer path between the point of application of magnetic forces and the noise radiating surface is relevant to effectively characterize the vibroacoustic behaviour. This paper focuses on the transfer path between the tip of stator teeth and the yoke outer surface. Thus the relevance of using FRF in modelling the mechanical response depends on the loading strategy. In particular, the unit-wave FRF (WFRF) and the tooth FRF (TFRF) are two methods used to model the response of an electrical machine to the magnetic force excitation [2]. In both methods a single magnetic Lumped Force (LF) per tooth is considered to load the structure.

The WFRF consists of loading all teeth at once with a spatial excitation of wavenumber n. The WFRF is generally performed using one LF per tooth [3]. The WFRF method allows to diagnose e-NVH sources based on the analytical analysis of the different electromagnetic sources [4]. However WFRF is hardly achievable through direct experimental measurement because in real electrical machines several wavenumbers generally coexist at a same frequency. On the other hand, the TFRF consists of loading a single tooth per simulation (or experiment), with generally a single load vector. The experimental Tooth FRF can be obtained by impacting a tooth with an impact hammer and measuring its external yoke vibration response with accelerometers normalized by the injected force. Hence the experimental cost is fairly reduced as the experiments only require to have the devices to perform experimental modal analyses (hammer and accelerometers).

This article proposes a new method which enables to generate an artificial WFRF based on TFRF measurement. This new method is called Tooth Wave FRF (TWFRF). The main interest of the TWFRF is to allow the import of experimental tooth response in order to numerically simulate the vibration and noise emitted by the machine during operation. In order to validate the method, this article presents the experimental protocol to measure TFRF on a testbench. The testbench was presented in [5]: it is designed to illustrate the interaction between magnetic forces and the structural response of electrical machines. The geometrical data of the studied stator are presented in Table 1 and in Fig. 1. The measurements and discussions are limited to radial excitations only.

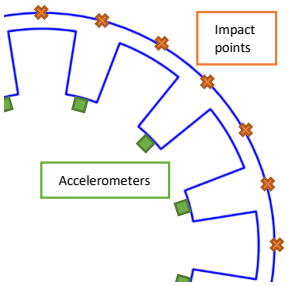

Figure 1. Benchmark 12s10p SPMSM for FRF Tooth measurement: $K_h = 24$ impact points evenly spaced on the yoke for $Z_s = 12$ tri-axis accelerometers (1 on each tooth tip).

Table 1. Parameters of the existing experimental prototype [5].

Parameter	**Symbol**	**Value**
Number of poles	p	10
Number of stator teeth	Z_s	12
Air gap length	g	2.5 [mm]
Slots per pole and per phase	spp	0.4
Rotation speed	N	0-5000 [RPM]
Stator lamination		M400-50A
Stator bore radius	R_{sbo}	48 [mm]
Stator yoke height	H_{sy}	5 [mm]
Stator tooth length	H_{tooth}	20 [mm]
Stator outer radius	R_{sy}	73 [mm]
Stator stack length	L_{st1}	140 [mm]
Stator slot width	W_s	18 [degrees]
Permanent magnet		NdFeB (N42)
Remanent flux density	B_r	1.28 [T]
Magnetic relative permeability	μ_{rm}	1.05
Maximum temperature	T_{max}	120 [°C]
Magnet width	W_{mag}	36 [°]
Magnet top radius	R_{mag}	45 [mm]
Magnet height	H_{mag}	5 [mm]
Magnet length	L_{mag}	70 [mm]
Rotor lamination		C22 (XC18)
Rotor bore radius	R_{rbo}	40 [mm]
Rotor shaft radius	R_{ry}	20 [mm]
Rotor length	L_{st2}	140 [mm]

2. Frequency Response Functions

2.1. Magnetic forces

This section presents the computation method of magnetic LF for the magneto-mechanical coupling. The method considers that the stator is excited with an air-gap radial Maxwell stress wave σ_r [3,6] computed on a circular contour on the stator bore radius R_{sbo} for the angular position $\alpha \in [0, 2\pi]$ at time t such that the force wave can be decomposed into:

$$\sigma_r(\alpha, t) = \sum_n \sum_\omega \sigma_r(n, \omega) e^{jn\alpha} \tag{1}$$

with j the imaginary number, ω the frequency, n the wavenumber. The next step is to integrate σ_r on a slot pitch $\frac{2\pi}{Z_s}$ to get $F_{r,i}$ which is the corresponding LF on

the i$^{\text{th}}$ tooth at angular position α_i:

$$F_{r,i}(t) = \int_{\alpha_i - \frac{\pi}{\mathrm{Z_s}}}^{\alpha_i + \frac{\pi}{\mathrm{Z_s}}} \sigma_{\mathrm{r}}(\alpha, t) \cos(\alpha_i - \alpha) \, \mathrm{d}\alpha \tag{2}$$

2.2. Wave Frequency Response Functions

This section presents the WFRF model with lumped tooth forces (LF). Assuming the mechanical linearity, each wavenumber n can be considered independently. Then the simulation of a limited number of spatial wavenumber allows to significantly reduce the computation time [2] and to understand the main source of magnetic noise [7]. Thus a single air-gap force wave amplitude is injected in (2) to get the corresponding spectral LF on the i$^{\text{th}}$ tooth at angular position α_i:

$$F_{r,i}(n, \omega) = \mathrm{R_{sbo}} \mathrm{L_{st1}} \frac{2}{n} \sin(n \frac{\pi}{\mathrm{Z_s}}) \sigma_{\mathrm{r}}(n, \omega) \mathrm{e}^{jn\alpha_i} \tag{3}$$

Then several harmonic FEA simulations are performed for each wavenumber n of interest with all teeth loaded according to (3). The injected amplitude is generally a unit air-gap stress wave $\sigma_{\mathrm{r}}(n, \omega) = \mathrm{e}^{j\omega + \phi_{n,\omega}}$ for a given range of frequency ω such that the output is normalized [3, 7]. The external yoke complex displacement per wavenumber $Y_{n,k}(\omega)$ is the output value of interest, with $k \in [1, \mathrm{K_h}]$ identifying a point on the radiating surface e.g. stator yoke.

2.3. Tooth Frequency Response Functions

The TFRF method is based on the linearity of the mechanical behaviour. Only one tooth is loaded per simulation with a normalized radial load $F_r(\omega) = \mathrm{e}^{j\omega}$. The number of simulations to be performed depends on the mechanical symmetry properties. For example, if the tooth pattern repeats itself over space such as in Fig. 1, only one simulation is necessary since all the teeth would have the same mechanical behaviour.

The TFRF can also be obtained experimentally by impacting a tooth with an impact hammer and measuring external yoke structural response with an accelerometer normalized by the injected force. The external yoke complex displacement per tooth $Y_{i,k}(\omega)$ is the output value of interest, with $i \in [1, \mathrm{Z_s}]$ identifying the tooth number and $k \in [1, \mathrm{K_h}]$ identifying a point on the radiating surface.

The immediate result of the TFRF is unsuitable for understanding the main sources of magnetic noise and vibrations. Indeed the electromagnetic components do not excite a particular region of the machine but rather in the form of a rotating force wave [7] such as (1). Thus Section 2.4 proposes to synthesize a WFRF from the results - experimental or numerical - of a TFRF.

2.4. Tooth Wave Frequency Response Functions

2.4.1. Methodology Principle

Considering the TFRF $Y_{i,k}(\omega)$ for $i \in [1, \mathrm{Z_s}]$ and $k \in [1, \mathrm{K_h}]$, the response to an air-gap sinusoidal excitation of wavenumber n is reconstructed a posteriori from the knowledge of (3):

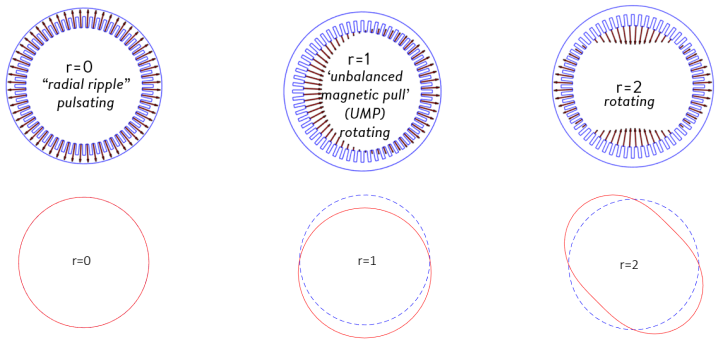

Figure 2. Lumped tooth force magnetic excitation depending on the wavenumber.

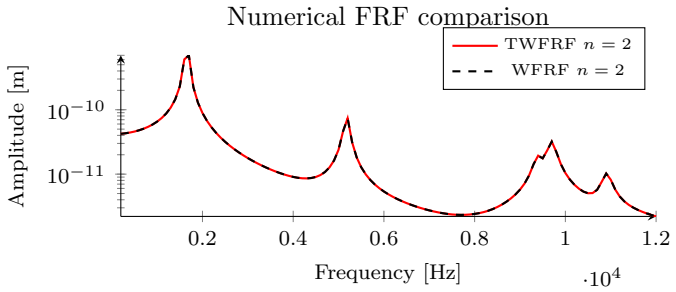

Figure 3. Comparison of numerical Frequency Response Functions (FRF): radial displacement RMS for unit-wave FRF (WFRF) method and wave FRF reconstruction from tooth FRF (TWFRF) method based on Finite Element Analysis.

$$Y_k(n,\omega) = \mathrm{R_{sbo}L_{st1}}\frac{2}{n}\sin(n\frac{\pi}{\mathrm{Z_s}})\sum_{i=1}^{i=Z_s} Y_{i,k}(\omega)\ \mathrm{e}^{jn\alpha_i} \tag{4}$$

The result $Y_k(n,\omega)$ called TWFRF is the displacement response to a unit force wave at a point k on the yoke surface. Thus, any excitation wavenumber can be artificially reproduced as illustrated in Fig. 2.

2.4.2. Purely Numerical Validation

A validation of the principle of the method is carried out using purely numerical results: a linear mechanical FEA is performed using MANATEE-Optistruct coupling on the same validation case as [2]. The results are presented in Fig. 3: as expected there is a perfect match between WFRF and TWFRF thanks to the mechanical linearity.

3. Experimental validation

3.1. Tooth Wave Frequency Response Function

The main interest of the TWFRF method comes from the compatibility with experimental measurements. It is an alternative to a complex and time-consuming modal analysis fitting of the FE model. Indeed, the previous TFRF can be measured experimentally on electrical machines. In this paper, the TFRF is measured between the tooth tip and the stator yoke. In the general case the methodology could be applied between the tooth tip and any noise radiating surface. The TFRF measurements can be performed using an impact hammer on the tip of the teeth while measuring the deflection on the yoke with an accelerometer.

Then the equivalent WFRF can be built using the previous TWFRF method. However, the impact area on tooth tip is more or less accessible depending on the topology. As a consequence, the mechanical reciprocity principle [1, 8] is introduced in the methodology to solve this last issue: impacting the tooth and measuring the yoke deflection can be equivalent to impacting the yoke and measuring the tooth deflection. If the measured radial displacement on the tooth number i after each impact on yoke's point k is denoted $Y_{k,i}(\omega)$, then according to the mechanical reciprocity principle:

$$Y_{i,k}(\omega) = Y_{k,i}(\omega) \tag{5}$$

This reciprocity principle assumes that the mechanical behaviour of the machine is linear, which is an acceptable assumption in the context of e-NVH. Hence the experimental protocol is much more feasible because a small accelerometer can be placed on the tooth tip and the external surface is much more accessible for the impact hammer. Thus, TFRF measurements are carried out with an accelerometer placed as in Fig. 1: the impact hammer is used on $\mathrm{K_h} = 24$ different points evenly spaced on the outer surface of the stator.

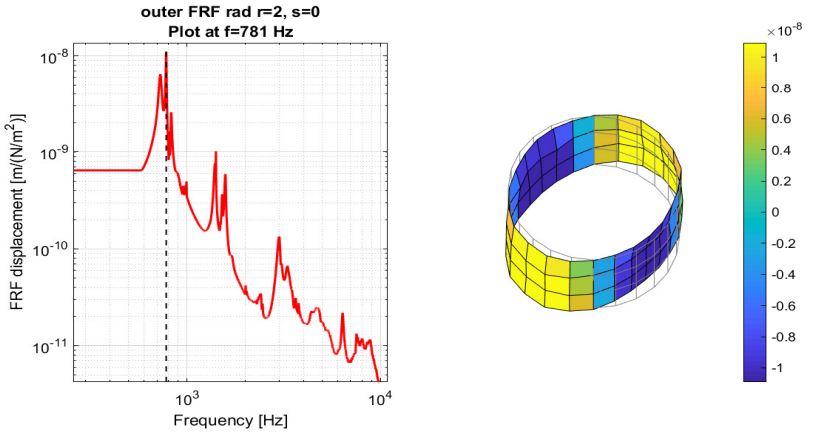

Figure 4. TWFRF for wavenumber r=2 generated with MANATEE from experimental data.

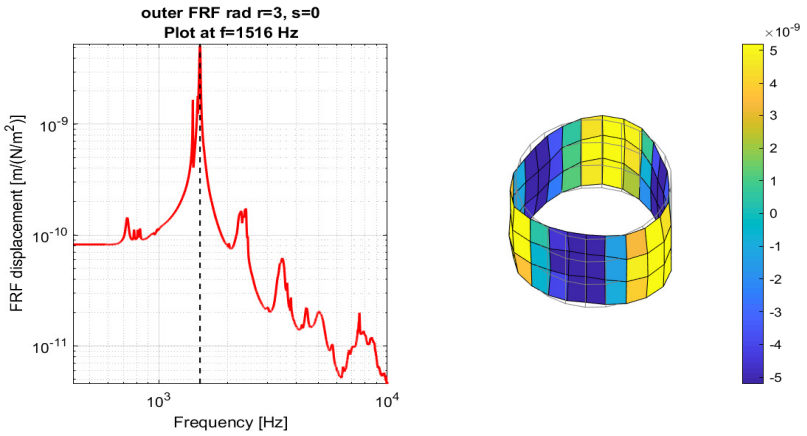

Figure 5. TWFRF for wavenumber r=3 generated with MANATEE from experimental data.

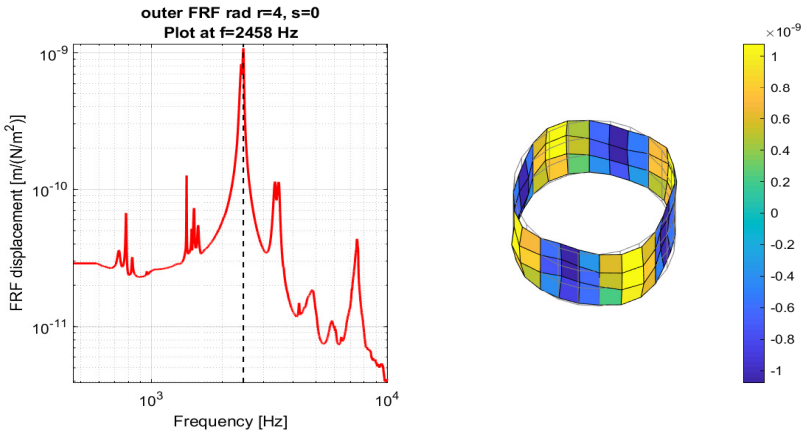

Figure 6. TWFRF for wavenumber r=4 generated with MANATEE from experimental data.

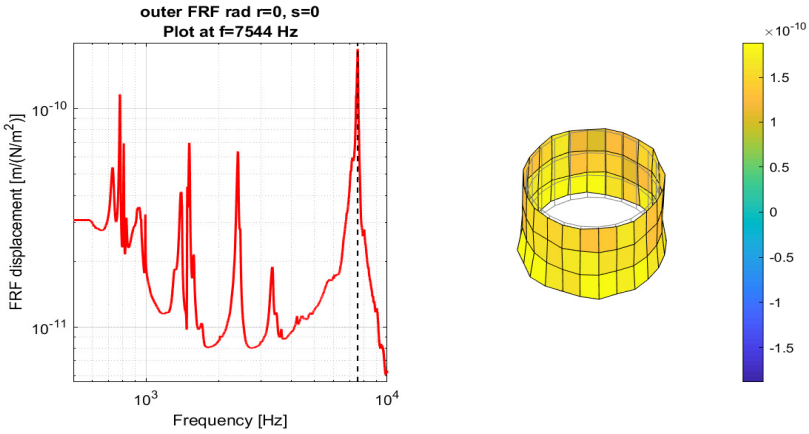

Figure 7. TWFRF for wavenumber r=0 generated with MANATEE from experimental data.

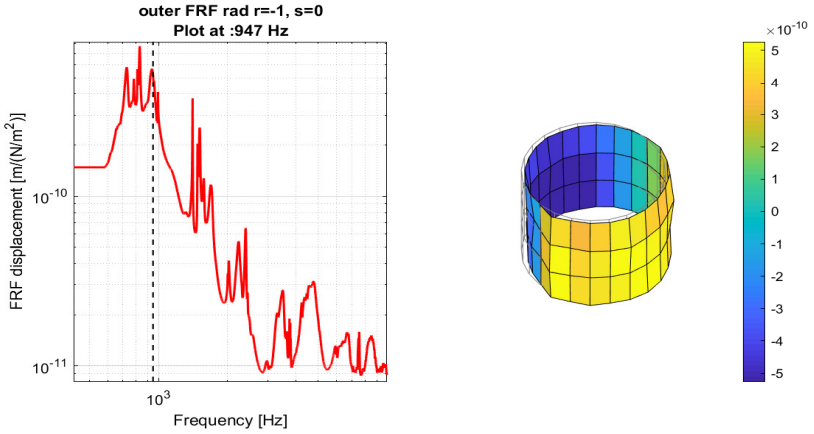

Figure 8. TWFRF for wavenumber r=1 generated with MANATEE from experimental data.

Once these measurements are carried out, the experimental displacement $Y_{k,i}$ is obtained. Then the TWFRF can be computed using (5) and (4). It leads to the results presented in Figs. 4-8: for each wavenumber, the displacement average amplitude is plotted next to the corresponding deformation map. To ease the reading, only the RMS value is plotted:

$$Y(n,\omega) = \sqrt{\sum_{i=1}^{\mathrm{K_h}} |Y_k(n,\omega)^2| / \mathrm{K_h}} \tag{6}$$

Another way to check the validity of the TWFRF method is to compare the frequency of the peak-value for each wavenumber with Experimental Modal Analysis (EMA). Note that the EMA was performed with the mounted rotor.

This comparison is performed in Table 2: it shows a good correlation suggesting that natural frequencies are correctly captured by the TFRF measurements. It means that the main electromagnetic noise phenomena - such as resonances - should be correctly modelized when applying the corresponding magnetic force wave amplitude.

Table 2. Comparison of experimental modes and TWFRF predicted resonance

Mode number	TWFRF	EMA (Ref)	Deviation
(0,0)	7544 [Hz]	7622 [Hz]	0.8 %
(2,0)	725 [Hz]	764 [Hz]	5.1 %
(2,0) bis	781 [Hz]	795 [Hz]	1.7 %
(1,0)	947 [Hz]	1087 [Hz]	12 %
(3,0)	1516 [Hz]	1570 [Hz]	3.4 %
(4,0)	2458 [Hz]	2531 [Hz]	2.9 %

Nevertheless, the discrepancy between the TWFRF and EMA may be influenced by the rotor mounting, in particular the bending/bounding modes such as $(1, 0)$. Indeed, the rotor have two ways to influence the benchmark mechanical behaviour: through the bearings, and through strong magneto-mechanical coupling as the magnets pulling force may influence the modal behaviour of the structure.

This could explains the larger deviation observed for mode (1, 0). The study of these particular effects will be the subject of future research work.

3.2. Run-up Acceleration from Simulation

The TWFRF is used as a mechanical input in a simulation performed with MANATEE software [9] in order to check the validity of the method. The vibration can be computed on all previous $\mathrm{K_h}$ points based on the electromagnetic simulation. The magnetic loads $\sigma_\mathrm{r}(n,\omega)$ are computed from (1) to be applied on the mechanical response to get the operational deflection spectrum RMS according to:

$$Y_{\mathrm{sim}}(\omega) = \sqrt{\sum_n \sum_m \sigma_\mathrm{r}(n,\omega)\sigma_\mathrm{r}^*(m,\omega) \sum_{i=1}^{\mathrm{K_h}} Y_k(n,\omega)Y_k^*(m,\omega)/\mathrm{K_h}} \tag{7}$$

where A^* is the complex conjugate of A. Note that (7) is equivalent to (6) when there is only one wavenumber n. As a consequence, $Y_n(\omega)$ is obtained by combining the previous experimental measurement (5) with the TWFRF reconstruction (4). This is called the TWFRF vibration synthesis. The computed magnetic spectrum is presented in Fig. 9.

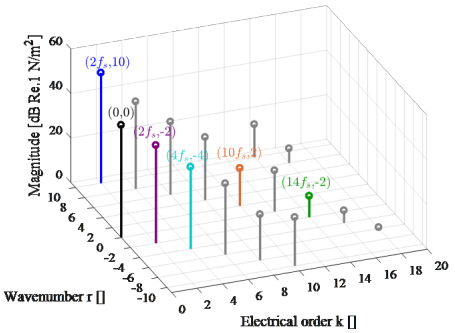

Figure 9. Main air gap stress harmonics of testbench PMSM machine [10]

Simulation and experimental results are presented under the form of a spectrogram in Fig. 10: the visible excitations correspond to harmonic content proportional to the synchronous frequency f_s:

$$f_s = p\frac{N}{60} \tag{8}$$

In particular, $2f_s$, $4f_s$ and $10f_s$ are the main excitations. The $2f_s$ and $4f_s$ excitations are below any natural frequency such that vibrations are only due to forced mechanical response. However the $10f_s$ excitations hits a natural frequency at 736 Hz and 892 RPM. It can be guessed from Table 2 that a resonance has occurred with mode (2,0). To a lesser extent, the (1,0) mode is excited by the $10f_s$ and the $8f_s$ around 1000 Hz.

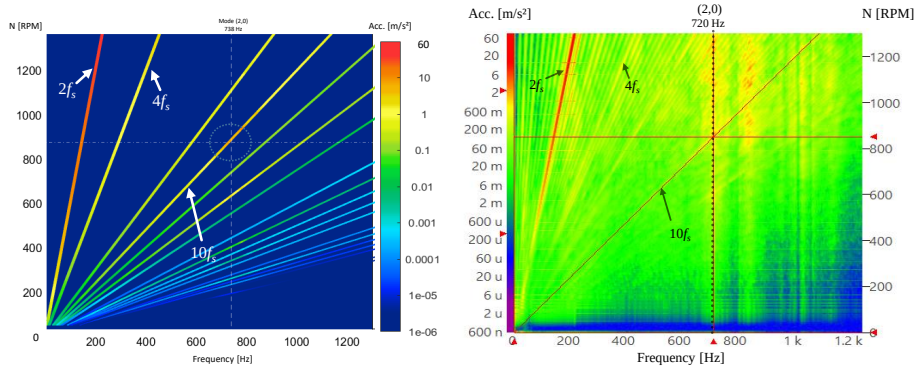

Figure 10. Spectrograms from TWFRF vibration synthesis (left) and from direct run-up measurement (right).

3.3. Run-up Acceleration from Experiments

3.3.1. Spectrogram

The goal of this section is to validate the previous predictions from the simulation based on TFRF measurements. For this purpose, the experimental acceleration spectrum is measured at various rotation speeds on the benchmark using the experimental setup presented in Fig. 11. All the details of the measurements are presented in [10].

Measurement results of one run-up are presented under the form of a spectrogram on the right side of Fig. 10 and it can be compared to the simulation on the left side. Indeed the main phenomena can be found back: the $2f_s$, $4f_s$ and $10f_s$ are again the main excitations, and the $10f_s$ excitation causes a resonance around 720 Hz at approximately 850 RPM. The excitation of the mode (1,0) is also visible around 850 Hz. However, the excitation of the mode (1,1) at 1150 Hz is not detected by the simulation because the current methodology does not consider 3D excitations. The extension to 3D should be the subject of another paper as it tackles complex issues such as skewing and non-uniform magnetic loads.

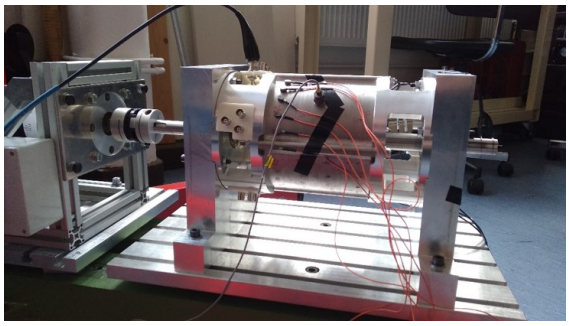

Figure 11. Experimental setup for acceleration measurements during run-up on the prototype 12s10p SPMSM

3.3.2. Order Tracking

In order to refine our comparison, the TWFRF based vibration synthesis is compared to direct measurement along an order of spectrograms from Fig. 11 and Fig. 10. The results are presented in Fig. 12 at $10f_s$ and in Fig. 13 at $2f_s$.

Both TWFRF vibration synthesis and direct run-up measurement have the same behaviour. The TWFRF simulation is overestimating the vibration level. The slight shift of the peaks probably comes from a difference between TWFRF predicted natural frequency and actual natural frequency. There are already some difference observed in Table 3, but additional differences might happened because of the run-up test conditions (temperature, mounted rotor, etc.).

First, the main e-NVH phenomenon that is observed is the resonance with the two different (2,0) modes in Fig. 12. Another resonance is observed for the run-up around 1077 rpm in Fig. 12 which is almost invisible with the TWFRF: it is assumed that it is the (1, 0) mode that is excited. Indeed the magnetic forces are computed with ideal excitations, missing the effect of eccentricities and unbalanced magnetization. In future research work, the air-gap magnetic flux density will be measured to adjust the magnetic force model.

Table 3. Comparison of mode excitation with rotation speed and frequency

Mode number	**TWFRF**		**Run-up**	
(2,0)	870 [rpm]	725 [Hz]	840 [rpm]	764 [Hz]
(2,0) bis	932 [rpm]	781 [Hz]	903 [rpm]	795 [Hz]
(1,0)	1147 [rpm]	955 [Hz]	1077 [rpm]	897 [Hz]

The comparison between run-up and TWFRF vibration synthesis could be further improved by taking into account unbalanced magnetization, eccentricities, rotor contribution to modes, longitudinal modes, and influence of temperature on natural frequencies (during the run-up the temperature of the benchmark has risen significantly). All these aspects will be the matter of future research works.

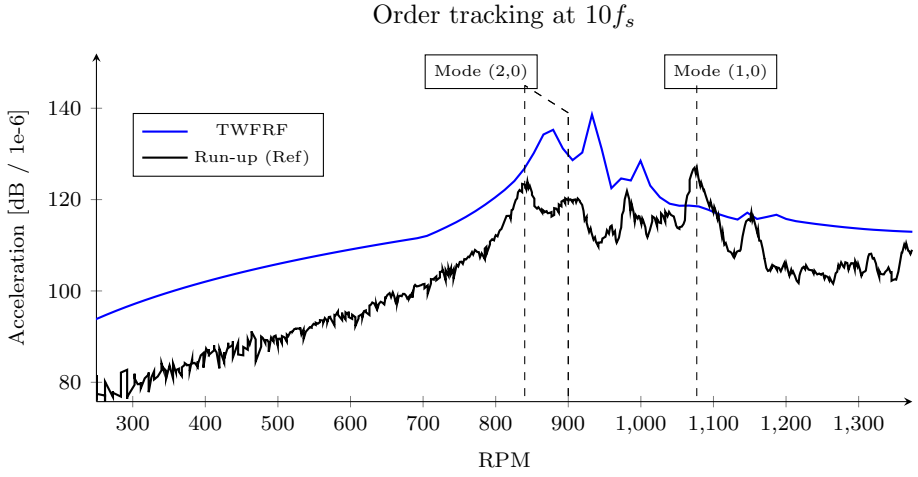

Figure 12. Comparison of the order tracking at $10f_s$ between the direct measurement of the acceleration during a run-up and the synthesized acceleration based on the TWFRF method.

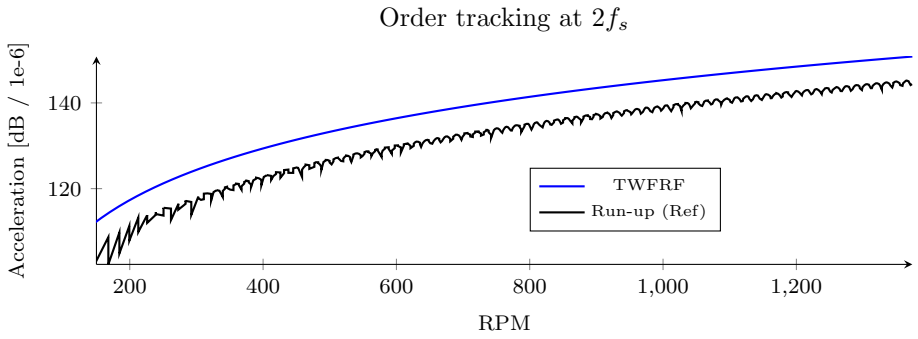

Figure 13. Comparison of the order tracking at $2f_s$ between the direct measurement of the acceleration during a run-up and the synthesized acceleration based on the TWFRF method.

4. Conclusion

In this paper, a new hybrid methodology has been proposed for the vibro-acoustic analysis of electrical machines under electromagnetic excitations. The goal of the paper is to prove that the methodology could be used to diagnose vibroacoustic behaviour of electrical machines.

The principle of the new TWFRF methodology is to reconstruct unit-wave FRF based on experimental measurements and to excite the structure with numerically computed magnetic forces. The measurements are performed under the form of single tooth FRF: an accelerometer is placed on the targeted tooth and the excitation is performed with an impact hammer on the external yoke. A new methodology is being applied to predict the corresponding unit-wave FRF based on the tooth FRF measurements. Indeed, physical electromagnetic excitations are rotating waves and standard excitation methods such as hammer or shakers can only create point excitations. By converting tooth FRF into wave FRF, more physical interpretations can be carried out.

Thus the mechanical response is characterized without any numerical FE simulations. The electromagnetic vibration response was synthesized by applying to each TWFRF the corresponding magnetic force wavenumber. The results are compared to experimental acceleration measurement at various speeds by using spectrograms. The comparison shows that the methodology based on TWFRF accurately predict the main 2D phenomena.

As a consequence, this methodology could be used to diagnose and troubleshoot electromagnetic noise issues. This new methodology is complementary to FEA, in particular for e-NVH optimization. This could be of great interest when considering complex systems such as structure borne noise in the passenger compartment of an electric vehicle. Future insights should concern:

- contribution of tangential forces;
- uncertainty due to experimental measurements (rotor contribution, eccentricities, etc.);
- extension to 3D noise issues, for example the excitation of longitudinal modes due to skewing; and
- extension of the method to FRF for sound pressure level per N/m^2.

References

[1] P. Avitabile, Experimental modal analysis, Sound and vibration 35 (1) (2001) 20–31.

[2] M. Régniez, Q. Souron, P. Bonneel, J. Le Besnerais, Numerical simulation of structural-borne vibrations due to electromagnetic forces in electric machines - coupling between altair optistruct and manatee software, Researchgate (2016).

[3] A. Saito, M. Kuroishi, H. Nakai, Vibration Prediction Method of Electric Machines by using Experimental Transfer Function and Magnetostatic Finite Element Analysis, Journal of Physics: Conference Series 744 (1) (2016) 012088. doi:10.1088/1742-6596/744/1/012088.

[4] W. Liang, The investigation of electromagnetic radial force and associated vibration in permanent magnet synchronous machines, Ph.D. thesis, Cranfield University (2017).

[5] E. Devillers, M. Hecquet, X. Cimetière, J.-P. Lecointe, J. Le Besnerais, T. Lubin, Experimental benchmark for magnetic noise and vibrations analysis in electrical machines, in: 2018 XIII International Conference on Electrical Machines (ICEM), 2018, pp. 745–751. doi:10.1109/ICELMACH.2018.8506928.

[6] R. Pile, E. Devillers, J. Le Besnerais, Comparison of Main Magnetic Force Computation Methods for Noise and Vibration Assessment in Electrical Machines, IEEE Trans. Magn. 54 (7) (2018) 1–13. doi:10.1109/TMAG.2018.2828388.

[7] M. Boesing, T. Schoenen, K. A. Kasper, R. W. De Doncker, Vibration Synthesis for Electrical Machines Based on Force Response Superposition, IEEE Trans. Magn. 46 (8) (2010) 2986–2989. doi:10.1109/TMAG.2010.2042291.

[8] K. Holland, F. Fahy, A guide to the exploitation of vibroacoustic reciprocity in noise control technology, ISVR Technical Report No 264 (1997).

[9] J. Le Besnerais, Fast prediction of variable-speed acoustic noise due to magnetic forces in electrical machines, in: 2016 XXII International Conference on Electrical Machines (ICEM), 2016, pp. 2259–2265. doi:10.1109/ICELMACH.2016.7732836.

[10] K. Degrendele, E. Devillers, J. Le Besnerais, Advanced nvh measurement data processing of electric motors under electromagnetic excitations, in: Automotive Acoustics Conference 2019, Springer, 2020, pp. 226–237. doi:10.1007/978-3-658-27669-0_16.